Sixth International Conference on Durability of Concrete Structures **Paper Number DDS03**
18 - 20 July 2018
University of Leeds, Leeds, West Yorkshire, LS2 9JT, United Kingdom

First Principles-Based Design of Economical Ultra-High Performance Concrete

A. Arora, M. Aguayo, F. Kianmofrad, Y. Yao, B. Mobasher and N. Neithalath
Arizona State University, Tempe, USA

ABSTRACT

This paper presents a novel strategy to design the binder phase of ultra-high performance concrete (UHPC) from commonly available cement replacement (fly ash, slag, microsilica, metakaolin) and fine filler (limestone) materials. A packing algorithm is used to extract the number density, mean centroidal distance, and coordination number of the microstructure. Similarly, rheological studies on the pastes provide yield stress, plastic viscosity, and mini-slump spread. The selection criteria involves using the three microstructural and three rheological parameters individually or in combination to define packing and flow coefficients. The selection criteria is flexible enough to allow users modify the constraints depending on the application. The binder with the desired packing and rheological features is combined with aggregate sizes and amounts chosen from a compressible packing model based on maximum packing density. A fiber volume fraction of 1% is also used, along with accommodations for wall and loosening effects. The model is programmed in a user-friendly environment to enable engineers select aggregates from locally available materials. Compressive strengths greater than 150 MPa are obtained for the selected UHPC mixtures after 28 days of moist curing. The strength-normalized cost of such mixtures is only a fraction of that of proprietary UHPCs.

Keywords: Ultra High-Performance Concrete; Microstructure; Rheology; Particle Packing; Compressive Strength; Durability

1.0 INTRODUCTION

Ultra-high performance concrete (UHPC) is an emerging cement-based material with high compressive and tensile strengths, ductility, and long-term durability (Graybeal, 2011; Russell and Graybeal, 2013; Wang *et al.*, 2012; Wille and Boisvert-Cotulio, 2015). Some of the applications for which UHPC is well suited for are bridge piers, decks and deck-level connections between modular precast components, blast protection elements, and tunnels (Graybeal, 2012; Maya and Graybeal, 2017; Tazarv and Saiidi, 2015; Vítek *et al.*, 2013). Compressive strengths in excess of 120-150 MPa are generally reported for UHPC mixtures (Graybeal, 2011; Yoo and Banthia, 2016), aided by careful selection of cementitious materials considering their particle sizes and reactivity, and a low water-to-powder ratio, w/p ($0.15 < w/b < 0.23$) to ensure a dense microstructure (Reda *et al.*, 1999). The use of non-standard cement replacement materials such as quartz (silica) flour, rice husk ash, and nanoparticles (nanosilica, nano-metakaolin) to achieve high strengths, in additional to common high-performance replacement materials such as silica fume and metakaolin, has been reported (Ghafari *et al.*, 2014, 2015; Huang *et al.*, 2017a; Li *et al.*, 2015b; Muhd Norhasri *et al.*, 2016; Shafieifar *et al.*, 2017; Van Tuan *et al.*, 2011). Limestone powder has also been used in several UHPC formulations (Arora, A. *et al.*; Burroughs *et al.*, 2017; Huang *et al.*, 2017b; Li *et al.*, 2015a). Recently, the use of calcium aluminate cement for UHPC has been explored, with a focus on high temperature applications (Lee *et al.*, 2017). Higher strength and durability are direct consequences of microstructure densification, while the use of discontinuous steel fibers (generally greater than 3% by volume) provides sustained post-cracking strengths and ductility (Le Hoang and Fehling, 2017).

The material design of UHPC binders is governed by an efficient particle packing process since the low w/p in these mixtures will result in sub-optimal levels of hydration of cement. High material costs and energy implications of UHPC can partly be attributed to the use of large amounts of cement that acts as an expensive filler. It is therefore well accepted that improved packing of the binder phase through the use of cement replacement materials and fine fillers is a better means of strength enhancement than increasing cement content. A recent work by the authors (Arora, A. *et al.*) has explained a methodology to design economical and efficient UHP binders that incorporate only conventional cement replacement materials (at an overall replacement level upwards of 30%), that achieves a high degree of microstructural packing and desirable rheology for flowable concrete. Similarly, the importance of aggregate packing to ensure desirable concrete properties has also been well documented. A well-designed aggregate component in mixtures such as UHPC also helps to

lower the cost, in addition to providing enhanced performance. Aggregate packing strategies to design UHPC mixtures have been reported (Chan and Kwan, 2014; de Larrard and Sedran, 1994; Soliman and Tagnit-Hamou, 2017; Yu *et al.*, 2014).

This paper implements a multi-scale design strategy to design UHPC mixtures by coupling the design of paste phase at the microstructure level and the aggregate phase at the mesostructure level. The design of UHP binder phase is based on microstructural packing-based and rheology-based criteria. Packing is a function of particle sizes and their distribution, while sizes and distribution along with particle surface characteristics influence the rheology. A microstructural packing algorithm is used to determine parameters relevant to particle packing. Yield stress, plastic viscosity, and mini-slump spread are used as the rheological parameters. This proposed method relies on the premise that, for low w/b concretes where only a fraction of the cement hydrates, (i) improved packing through the use of cement replacement materials and fine fillers is a better means of strength enhancement than increasing cement content, and (ii) better rheology helps better dispersion of the grains, aiding in mixture placement as well as hydration in the presence of low amounts of water, and consequently better mechanical properties.

The design for the optimum aggregate gradation is based on the compressible packing model (De Larrard, 1999; Roquier, 2016), Contrary to many UHPC mixtures that contain only fine aggregates, the material design reported in this paper considers coarse aggregates (passing 9.5 mm sieve) also. The mechanical strengths and durability performance of the designed UHPC mixtures are also reported. The methodology is designed in such a manner to be implemented in a computer program to optimize the UHPC mixtures from both the performance and cost perspectives.

2.0 MATERIALS AND METHODS

2.1 Materials

The components of the binder phase of UHPC mixtures studied here include a Type I/II ordinary portland cement (OPC) conforming to ASTM C 150, Class F fly ash and metakaolin conforming to ASTM C 618, ground granulated blast furnace slag (GGBFS) conforming to ASTM C 989, limestone powder conforming to ASTM C 568, and micro silica (silica fume) conforming to ASTM C 1240. Limestone powders with two different median particle sizes (1.5 µm and 3.0 µm) are used to ensure improved particle packing. The particle size distribution (PSD) curves of the powders are shown in Fig. 1, while their chemical compositions and physical characteristics are shown in Table 1. The water-to-powder ratios (w/p) varied between 0.165 and 0.20 depending on the starting materials used. A polycarboxylate ether (PCE)-based superplasticizer was used. The ratio of solids content of the superplasticizer to the binder content was maintained between 1% and 2%. Fine and coarse aggregates conforming to ASTM C 33 were used. Smaller coarse aggregates are required to proportion UHPC mixtures, and thus only those passing a 3/8" sieve (9.5 mm) was used.

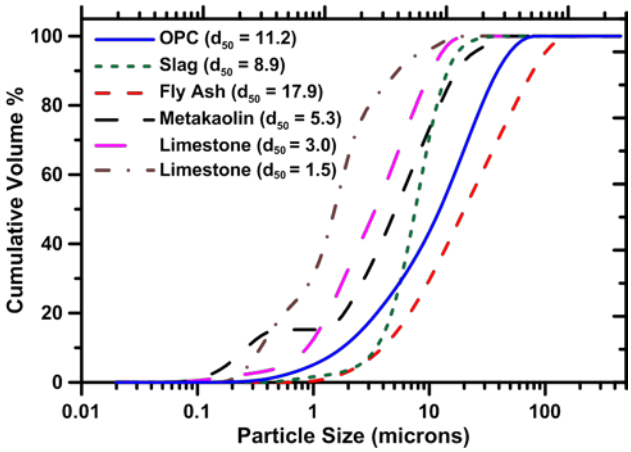

Fig. 1. Particle size distribution curves for cement, fly ash, slag, metakaolin, and limestone powders. The median size in microns is shown in parentheses.

Table 1. Chemical composition of the starting materials used for the binders in this study

Components of the binder	SiO_2	Al_2O_3	Fe_2O_3	CaO	MgO	SO_3	LOI
OPC	19.60	4.09	3.39	63.21	3.37	3.17	2.54
Slag (S)	39.41	8.49	0.37	35.53	12.05	2.83	1.31
Fly Ash (F)	58.40	23.80	4.19	7.32	1.11	3.04	2.13
Metakaolin (K)	51.70	43.20	0.50	-	-	-	0.16
Micro silica (M)	> 90.0	-	-	< 1.0	-	-	-
Limestone (L), 1.5 µm	> 97% $CaCO_3$						
Limestone (L), 3 µm							

The aggregates were then classified into three nominal maximum sizes: ¼" (6.25 mm), #4 (4.75 mm), and #8 (2.36 mm). Since the procured aggregates contained a dominant portion of 6.25 mm particles, they were crushed using a laboratory

pulverizer to obtain the requisite amounts of 4.75 mm and 2.36 mm size particles. The aggregates were washed and dried to remove impurities on the surface that might interfere with water demand and strength. The bulk specific gravity and absorption of the aggregates were determined as 2.65 g/cc and 0.94% respectively. Coarse and fine silica sands were used as fine aggregates, which had median sizes of 0.6 mm and 0.2 mm respectively. The mortar mixtures had both sand types in equal amounts. The mortar cubes and the cylindrical concrete specimens were proportioned using a paste volume fraction of 65%. The fiber reinforced UHPCs employed straight high-strength steel microfibers having a length of 13 mm and a diameter of 0.5 mm. The aggregates and fibers used are shown in Fig. 2.

Fig. 2. Coarse aggregates (6.25mm, 4.75mm and 2.36mm), fine aggregates (coarse sand, fine sand) and steel fibers used in the study.

2.2 Mixing and Curing Procedure

All dry powders were thoroughly mixed prior to wet mixing. Paste mixing was performed in accordance with ASTM C 1738 using a M7000 high speed shear mixer. The following mixing sequence was used: (i) all water and HRWR was added to the mixer, (ii) the blended dry powders were then added as the mixer was run at 4000 rpm for approximately 30 s, (iii) the mixer was then run at 12,000 rpm for 30 s, (iv) the paste was allowed to rest for two minutes, and (v) final mixing of the paste was carried out at 12,000 rpm for 90 s.

Concrete was mixed in a a mixing bucket made of HDPE. A 12.5 mm Dewalt^{TM} spade drill attached to a spiral drill bit was used as the mixing tool for better shearing of particles. This is required to disperse the finer components of the binder – micro-silica and metakaolin in particular. Coarse and fine aggregates were initially blended together. If the aggregates were dry, mixing water corresponding to their absorption values was added. The aggregates were then blended with micro-silica for 5 minutes. This allowed for shearing between the hard quartz particles and micro-silica to de-agglomerate the micro-silica particles and disperse them adequately. Next, limestone powder was added and mixed until it was uniformly dispersed in the mixture. Fly ash or slag and OPC were subsequently added and mixed for a minimum of 3 minutes until the mixture became homogenous. After all the dry powders and fine aggregate were mixed, half the amounts of desired mixing water and superplasticizer were added and mixed for another 5 minutes. Care was taken to ensure that the mixture does not adhere to the sides of the mixer. The remaining water and superplasticizer was added and mixing was continued for an additional 5 minutes. The final stage of mixing lasted between 5-10 minutes (depending on the type of the mixture) until the mixture became very fluid and cohesive. In the case of fiber reinforced UHPC, fibers were slowly added during the final stage of mixing.

2.3 Test Methods

The rheological characteristics of all the pastes were determined using TA instruments AR 2000EX rotational rheometer with a vane in cup geometry. This geometry eliminates issues with slip in rheological measurements. All experiments were carried out with the set up maintained at a temperature of 25 ± 0.1 °C. Approximately 40 mL of paste is placed in the rheometer geometry using a disposable syringe. The amount of time between the addition of mixing water and beginning the rheological experiment was approximately 5 min. The yield stress and plastic viscosity of all the pastes was evaluated using a strain-rate controlled experiment. The rheological procedure consisted of a ramp-up pre-shear phase from 10-to-100/s lasting around 75 s to homogenize the paste, followed immediately by a ramp-down to 0.005/s. This phase is followed by a ramp-up phase from 0.005-to-100/s, and a ramp-down phase from 100-to-0.005/s. Fig. 2(a) graphically represents this procedure. Excluding the pre-shear phase, data is acquired every second until three consecutive torque measurements are within 8% of each other, at which time the experiment advances to the next shear rate.

The compressive strength of 50 mm mortar cubes was determined in accordance with ASTM C 109 and that of the 75 mm x 150 mm cylindrical concrete specimens in accordance with ASTM C 39. The paste volume fraction in the mortars was maintained at 65%. The flexural response of the specimens after 28 days of curing was evaluated using four-point bending tests in accordance with ASTM C 1609 in a closed-loop, servo-controlled testing system. Prismatic concrete beam specimens (50 mm x 65 mm x 380 mm) were tested in flexure. Six beams were tested for each mixture.

The resistance of UHPC to chloride ion penetration was measured using the Rapid Chloride Permeability test (RCPT, ASTM C 1202) and Non-Steady State Migration test (NSSM, NT Build 492). Both tests are

carried out on concrete discs 100 mm diameter and 50 mm long, cut from 200 mm long cylinders.

3.0 STRATEGIES FOR DESIGNING THE IDEAL PASTE PHASE

Binary, ternary and quaternary blends were proportioned by mixing different amounts of these replacement materials with OPC. The total cement replacement level generally varied between 20 and 30% by mass of OPC. Binary mixtures consisted of commonly employed cement replacement materials including fly ash, slag, micro silica or metakaolin. In the ternary and quaternary blends, the replacement levels of fly ash or slag were varied between 10 and 25%, while those of silica fume or metakaolin were varied between 7.5 and 10%. Fly ash or slag were considered to be the primary cement replacement materials in ternary and quaternary blends because of their abundance and the larger OPC replacement levels that can be accomplished. Limits to the amounts of micro silica and metakaolin were necessary to ensure adequate dispersion of these materials within the paste. Limestone powders of two different median sizes, either individually, or in equal parts, were used to supplement the binary and ternary mixtures with even finer sizes that they were deficient in, to enhance particle packing. The limestone content varied between 5 and 10%.

Table 2 shows the proportions of all the 33 different mixtures (one UHP-control, one HP-control, and 31 UHP pastes) evaluated in the initial phase of this work. All the ultra-high performance (UHP) pastes were proportioned using a volumetric water-to-powder ratio, $(w/p)_v$, of 0.63 (corresponding to a mass-based $(w/p)_m$ of 0.20; 0.22 when the water in the HRWR is also added). In addition to the control UHP paste ($(w/p)_m$ of 0.20), a high performance OPC paste with a $(w/p)_m$ of 0.32 was also proportioned. A commercially available high range water reducer (HRWR) (Master Glenium 7500, manufactured by BASF) was used at a solids content of 1.25% by mass of the powder to improve the workability of the UHP pastes. In Table 2, UHP-control refers to the control mixture made using OPC alone and a $(w/c)_m$ of 0.20, and HP-control refers to the mixture made using a $(w/c)_m$ of 0.32.The HRWR dosage for the HP-control mixture was 2% by mass of the powder.

From a large matrix of paste mixtures (Table 2), a smaller sub-set needs to be chosen for detailed studies. In this study, a comprehensive method of binder selection is adopted, which relies on a combination of computational microstructural packing and experimental paste rheology, along with considerations for maximizing OPC replacement. This methodology eliminates the traditional trial-and-error method of mixture design for UHP binders, and provides a rational process to select candidate mixtures from a large set of potential raw materials.

Table 2. Mixture proportions for pastes evaluated in this study. All the pastes except HP-Control were proportioned using a (w/p)m of 0.20.

Mixture composition	Replacement material (% by mass of cement)			
	Fly Ash (F)/ Slag (S)	Metakaolin (K)	Microsilica (M)	Limestone (L); d_{50} of 1.5 or 3 µm[#]
UHP-control	0	0	0	0
HP-control	0	0	0	0
OPC + F/S	20, 30	0	0	0
OPC + M	0	0	10, 20	0
OPC + K	0	10	0	0
OPC + F/S + M	10, 20	0	10	0
OPC + F/S + K	10, 20	10	0	0
OPC + F/S + L	20	0	0	10a, 10b
OPC + F/S + L	25	0	0	5a, 5b
OPC + F/S + M + L	17.5	0	7.5	5b,5c
OPC + F/S + K + L	17.5	7.5	0	5b,5c

[#]The subscripts ‘a’, ’b’ and ‘c’ along with the dosage of limestone powder indicate the type of limestone used in the mixture: ‘a’ – 1.5 µm limestone, ‘b’ – 3 µm limestone and ‘c’ – 50% 1.5 µm + 50% 3 µm limestone.

3.1 Microstructural Packing

Microstructural models were created for all the paste mixtures in the study to analyze the particle contacts and inter-particle interactions. For this purpose, a random packing program was developed in MATLAB® to create virtual 3-D microstructures for different paste compositions. The total volume of particles in the RVE (representative volume element, chosen here as 300 x 300 x 300 μm^3) is determined based on the $(w/p)_v$. The cumulative particle size distributions of the component powders (Fig. 1) were discretized to obtain the number of particles of the individual components required to satisfy the desired solid volume fraction. Fig. 4 shows a representative virtual 3D microstructure corresponding to a quaternary mixture.

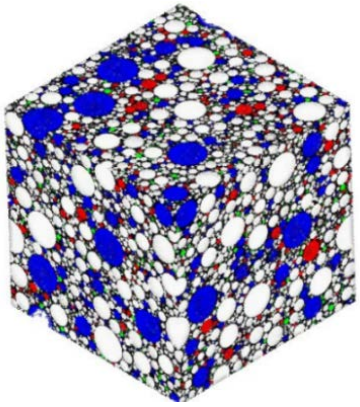

Fig. 4. Representative volume element (RVE) for a quaternary system containing OPC, fly ash, metakaolin and limestone. OPC is indicated in white, fly ash in blue, metakaolin in red, and limestone in green

The mean centroidal distance, coordination number and the number density are the key parameters that can be extracted from the analysis of the virtual RVEs. The mean centroidal distance is a measure of the packing density of the microstructure. It is calculated as the average distance to the center of a particle from the centroid of the microstructure. The coordination number is defined as the average number of nearest neighbor pairs in the microstructure. For any particle, the nearest neighbor is defined as a particle that lies either wholly or partially in the radial field of that particle, defined as a field with a radius of (r+5) µm, where 'r' is the radius of the particle. The number density is defined as the number of particles in a unit volume. It is directly related to the overall fineness of the powders in the paste. Other parameters, similar in nature to those represented here (e.g., particle contact fraction, which is similar to CN) have been used in the past to define the microstructure (Arora *et al.*, 2016; Vance *et al.*, 2015).

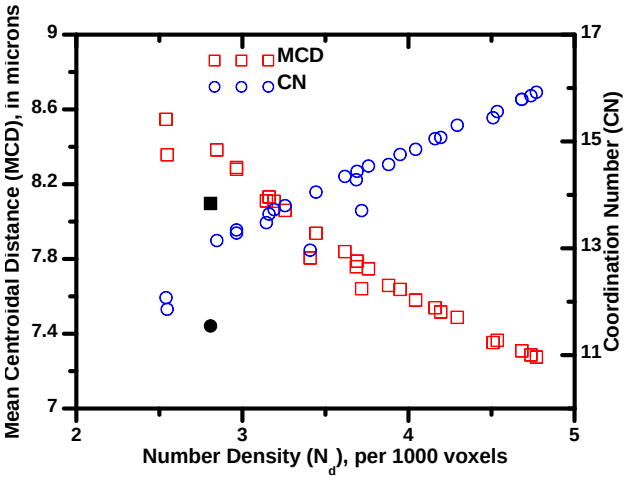

Fig. 5. Relationships between the number density, mean centroidal distance and coordination number for the UHP pastes. The values for the UHP-control paste are shown using filled symbols.

Figure 5 shows the relationships between the microstructural parameters of the UHP pastes. As the number density increases, the mean centroidal spacing between the particles decreases and the coordination number increases. The coordination number as well as the number density indicates the interparticle contacts in the microstructure and thus can be related to the yield stress of the paste and its degree of hydration at early ages. Moreover, plastic viscosity has been stated to be dependent heavily on the solid volume fraction (and thus the surface contacts) in the paste, thereby relating to the above-mentioned parameters. These microstructural parameters can therefore be considered to influence both the rheology and hydration in cementitious materials.

3.2 Rheological Parameters

Rheological studies of cementitious suspensions provide an understanding of how these materials behave in the fresh state and serve to monitor structure development that dictates the development of the mechanical properties. The plastic viscosity of fluid suspensions is considered to be primarily influenced by inter-particle friction and surface contacts, wherein decreasing the inter-particle (friction) forces by increasing particle spacing (or by decreasing surface contacts) results in a decrease in plastic viscosity. The yield stress is a more complex parameter, defined as the non-zero (finite) stress at a "zero" strain rate. A simpler way to characterize the flowability of cementitious suspensions is the mini-slump test which measures the area of spread of the fresh paste. The tests are carried out as described in the previous section. Fig. 6(a) and 6 (b) show the yield stress, plastic viscosity, and the normalized mini-slump spread area (A_{ms}) for all the pastes in which fly ash and slag respectively are the dominant cement replacement materials. The areas of the mini-slump spread are shown by normalizing them with respect to the spread area for the UHP-control paste. The numbers as subscripts in the mixture labels indicate the OPC replacement level with that material.

It is observed from Fig. 6(a) and 6 (b) that the yield stress values are directly related to the plastic viscosity values for all the paste mixtures, with an increase in one causing the other also to increase, even if not proportionally. The mini-slump values are noted to be inversely related to yield stress and plastic viscosity. It can also be noticed that the binary pastes containing fly ash or slag demonstrate relatively lower yield stress and plastic viscosity values as compared to the UHP-control paste. This is due to the lower inter-particle frictional forces in these pastes; a result of particle sizes and surface characteristics. It is also seen that the ternary mixes containing metakaolin show high yield stress values; however, incorporation of fine limestone reduces the yield stress in quaternary mixtures. The presence of fine limestone improves the overall packing and reduces the inter-particle friction in the quaternary

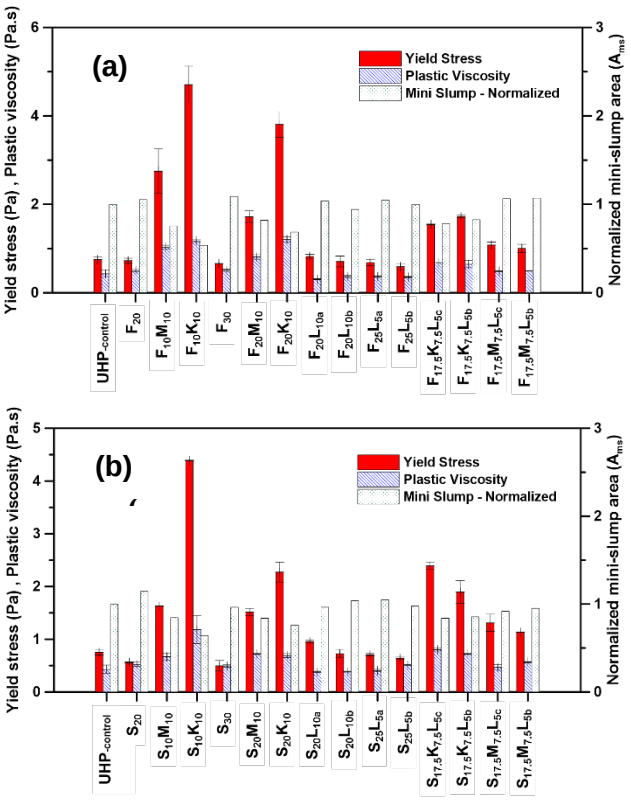

Fig. 6. Yield stress, plastic viscosity and normalized mini slump values for pastes containing: (a) fly ash as the primary cement replacement material, and (b) slag as the primary cement replacement material. The subscript numbers represent the % by mass of the corresponding material replacing cement.

mixtures thus lowering the yield stress and plastic viscosity, thereby leading to increased flowability of these mixtures (Vance *et al.*, 2013; Vikan and Justnes, 2007).

3.3 Selection Criteria Based on Microstructural and Rheological Parameters

Figure 7 shows a schematic of the algorithm for binder selection based on the microstructural and rheological parameters. The third step in Fig. 7(a) and 7(b) illustrates the selection criteria using these parameters individually, or their combinations (packing and flow coefficients) to select a smaller sub-set of binders from the ones shown in Table 2. The criteria for microstructural packing is defined in Fig. 7(a) such that the selected binder demonstrates a higher degree of packing as compared to the control UHP binder, which is used as the baseline case. The criteria for flowability is defined in Fig. 7(b) such that the selected binder has an acceptable level of workability as compared to the control UHP binder. Two strategies (Model 1 and Model 2) are presented for preliminary evaluation of the 31 binders in Table 2 in terms of their suitability to be considered as ultra-high performance binders. Model 1 considers a straightforward approach and compares the individual microstructure and rheological parameters with the respective UHP parameters. From the previous section, it is obvious that that a lower mean centroidal distance, a higher coordination number, and a higher number density will lead to a densely packed microstructure. Along with that, a workable mixture will have a lower yield stress and plastic viscosity and a higher mini-slump spread. Thus, the potential UHP binder should satisfy all the three rheology criteria. It should be noted here, however that the constants used as multipliers for the UHP control parameters in Model 1 are user-defined constants and may be changed depending on the packing and workability requirements for the specific application.

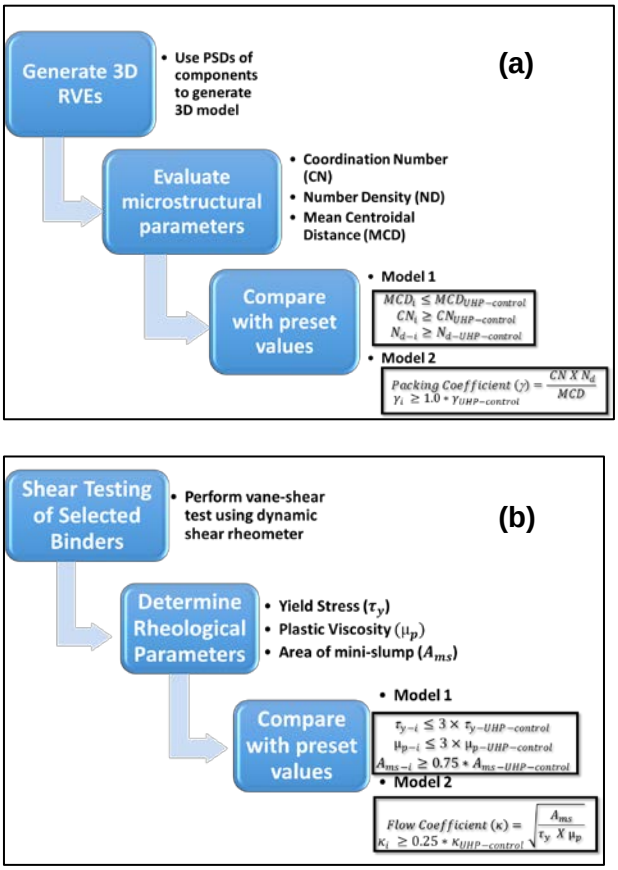

Fig. 7. Binder selection strategy based on: (a) microstructural parameters (coordination number, number density and mean centroidal distance) from virtual RVEs, and (b) rheological parameters (yield stress, plastic viscosity and area of mini slump)

Figures 8(a) and 8(b) show the Venn diagrams depicting the number of mixtures that satisfy the individual microstructural packing and rheology criteria respectively, as discussed in Model 1. From Fig. 8(a), it can be seen that 30 mixtures satisfy the CN and ND criteria while 24 satisfy the MCD criterion. 22 of the 31 UHP mixtures satisfied all the three packing criteria, and 23 of the 31 mixtures satisfied all the rheology criteria. Figure 8(c) shows that 17 mixtures satisfied both the packing- and rheology-based criteria. These criteria can be modified to further refine the mixture selection, as mentioned earlier. Figure 8 shows the matrix of 31 mixtures among which the selected ones are highlighted.

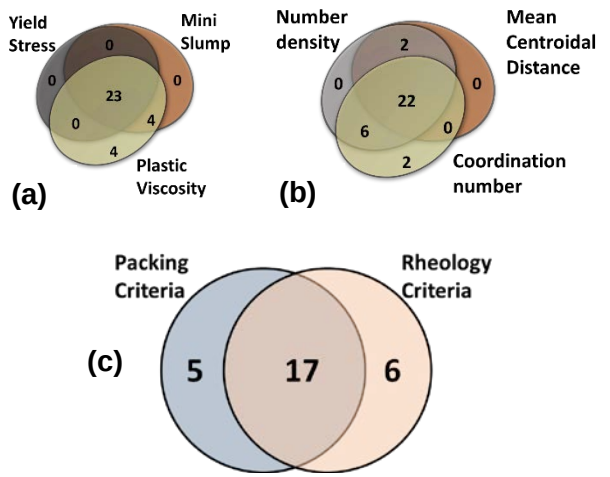

Fig. 8. Venn diagrams showing the number of mixtures selected based on: (a) microstructural criteria, (b) rheology criteria, and (c) the intersection of both the criteria. Note that Venn diagrams could not be drawn to scale because of the presence of zeros.

Model 2 combines the rheological and microstructural parameters to calculate flow and packing coefficients for evaluating the rheological and microstructural response respectively of each preliminary mix design. The values for both the packing and flow coefficient are normalized with respect to the parameters obtained for the control UHP binder. A higher value for γ indicates better packing whereas a higher value for κ indicates better workability for the UHP paste. Similar to the discussion above, the constant multipliers (1.0 for γ and 0.25 for κ) are user-defined and enable the user to have control over the selection of binder based on the desired application. Hereafter, we again select those binders that satisfy both the packing and flow criteria. It was found that out of the 31 UHP binders, 23 satisfied the packing criterion, and 28 satisfied the flow criterion. 22 binders satisfied both the criteria, and 8 among those were selected for further evaluation (Fig. 9).

K_{10}	M_{10}	M_{20}	F_{20}	F_{30}	S_{20}	S_{30}	
$F_{10}K_{10}$	$F_{20}K_{10}$	$S_{10}K_{10}$	$S_{20}K_{10}$	$F_{10}M_{10}$	$F_{20}M_{10}$	$S_{10}M_{10}$	$S_{20}M_{10}$
$F_{20}L_{10a}$	$F_{20}L_{10b}$	$F_{25}L_{5a}$	$F_{25}L_{5c}$	$S_{20}L_{10a}$	$S_{20}L_{10b}$	$S_{25}L_{5a}$	$S_{25}L_{5b}$
$F_{17.5}K_{7.5}L_{5b}$	$F_{17.5}K_{7.5}L_{5c}$	$F_{17.5}M_{7.5}L_{5b}$	$F_{17.5}M_{7.5}L_{5c}$	$S_{17.5}K_{7.5}L_{5b}$	$S_{17.5}K_{7.5}L_{5c}$	$S_{17.5}M_{7.5}L_{5b}$	$S_{17.5}M_{7.5}L_{5c}$

Fig. 9. Matrix of mixtures with the highlighted cells showing the mixtures selected based on packing and flow coefficients. Mixtures in the dark shaded cells were chosen for detailed studies

The selection of eight binders was based on the relative chemical compositions and reactivity of the components. For instance, (i) only ternary and quaternary binders are considered because of their better packing, with limestone included only in the quaternary binders, (ii) a total cement replacement level of 30% is used to ensure sustainable UHP binders, (iii) limestone is considered only in binders containing metakaolin or microsilica since its size range is in between those of fly ash/slag and microsilica/metakaolin, and its low reactivity (Vance *et al.*, 2013) limits the dosage to 5% (even though a recent study has shown increasing strengths with increasing limestone content in UHPC (Huang *et al.*, 2017b)), and (iv) when limestone is used, equal proportions of those with d_{50} values of 1.5 µm and 3 µm are preferred for improved packing.

3.4 Compressive Strength Development of Selected Binders

Compressive strength testing was carried out on 50 mm cubes cast for all the eight selected binders after 14 and 28 days of moist curing (Fig. 10). The mass-based water to binder ratio was kept constant at 0.22 and the HRWR dosage was maintained at 1.25% (solids content). The volume fraction of paste in these mortars was kept at 50%. A regular high-performance plain cement mortar (w/c = 0.32) was also formulated for comparison. It is observed that even with a clinker factor reduction of 30%, most of the UHP mortars, especially the quaternary blends demonstrate 28-day strengths that are comparable to, or higher than that of the control UHP mortar. The mixtures containing slag demonstrate higher strengths than those containing fly ash at 28 days, but it is conceivable that the pozzolanic reaction of fly ash and its later synergy with the other replacement materials could improve the strength with further curing. It is noted that the addition of fibers, reduction of water to binder ratio, optimization of the aggregate size fractions would lead to a final mixture with 28-day compressive strengths in excess of 150 MPa.

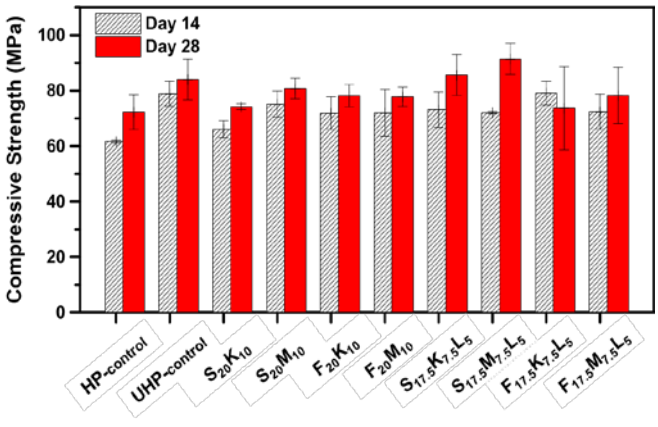

Fig. 10. 14-day and 28-day compressive strengths of selected UHP mortars. Error bars indicate one standard deviation from the average of at least three replicate specimens

4.0 DESIGN OPTIMIZATION FOR CONCRETE

Out of the eight binders selected for compressive strength analysis in the previous section, two binders were chosen based on their 28-day compressive strength, clinker factor and economical value. A third binder consisting of a ternary blend of cement, silica fume, and limestone with an overall cement replacement of 50% by mass, was also considered for further evaluation. The selected binder compositions are given in Table 3. The w/p ratio was lowered for these mixture from 0.22 to less than 0.20 by using high shear mixing procedure as detailed before and by increasing the amount of HRWR dosage. The mixtures were initially composed of a low w/p, and then small amounts of water and superplasticizer were added in stages to achieve the desired workability. Hence the w/p and superplasticizer dosage are different for the three mixtures. It is noted that the mixture containing fly ash as the dominant cement replacement material required the least amount of water and superplasticizer for desired workability, owing to the spherical nature of these particles.

Table 3. Selected binders and their compositions

Mixture ID*	Replacement material (% by mass of cement)				w/p	HRWR (% solids content by mass of the binder)
	F/S	K	M	L**		
$S_{17.5}M_{7.5}L_5$	17.5	0	7.5	5	0.194	1.5
$F_{17.5}M_{7.5}L_5$	17.5	7.5	0	5	0.166	1.2
$M_{20}L_{30}$	0	0	20	30	0.188	1.4

* The mixtures containing fibers are labeled in the graphs with '-f' after the mixture ID specified in this table.

** Equal amounts of limestone powder with d_{50} of 3 µm and 1.5 µm are used in these mixtures.

4.1 Compressive Strength

Mortars were cast using the mixture proportions reported in Table 3. The fine aggregate used was an equal mixture of coarse sand (d_{50} = 0.6 mm) and fine sand (d_{50} = 0.2 mm) since this combination was found to provide better strengths for several trial mixtures. The volumetric ratio of paste-to-aggregate was selected to be 0.65:0.35, again based on better strength results that were obtained for this combination as opposed to a 0.50:0.50 paste-to-aggregate ratio that was employed in several trial mixtures. The mixing procedure as specified earlier was followed to cast 75 mm x 150 mm cylinders.

Figure 11 shows the compressive strengths of these mortars determined in accordance with ASTM C 109, as a function of the age since casting. At 90 days, all

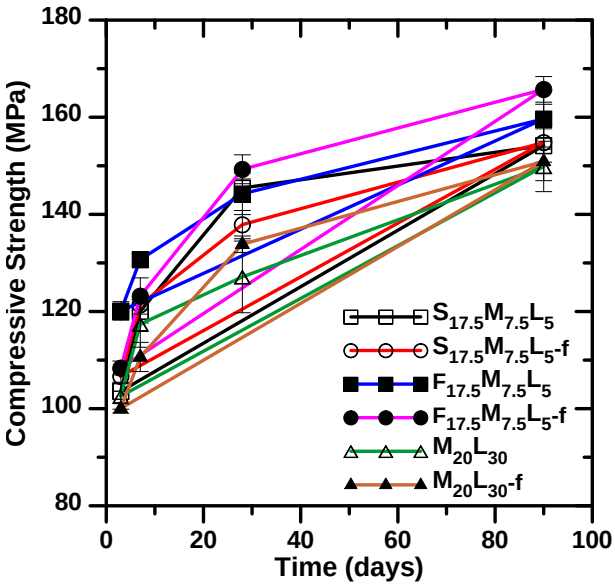

Fig. 11. Compressive strength of UHP mortar samples as a function of age.

the mixtures are found to attain a compressive strength of 150 MPa or higher, with the quaternary fly ash-based mixture showing the highest strength. Better workability of the mixture, along with a lower w/p contributed to this response. Even with a 50% clinker factor reduction, the ternary silica fume-limestone blend shows a 90-day strength of 150 MPa.

4.2 Particle Packing Based Design of UHPC

Mortars exhibiting ultra-high strengths beyond 150 MPa were designed using the paste selection strategy discussed in the previous sections. Following this, the mixture proportioning approach for UHPC must also ensure appropriate selection of the aggregate phases in addition to having the ideal paste phase. The selection of aggregates is governed by aggregate packing at the meso-scale since average aggregate sizes are about 100 times larger than the average sizes of the powders in the pastes. The use of a proper size distribution of aggregate particles can help increase the overall packing density of the concrete mixture in combination with the use of a properly chosen paste phase.

The current study uses a compressible packing model (Stovall *et al.*, 1986) to calculate the packing density of a mixture consisting of different volume proportions of aggregates. The compressible packing model for multi-sized grains expresses the packing density as a function of the fractional solid volume of each size of grain present. A compaction index 'K' is defined, which is a scalar index that takes a value based on the physical process used for aggregate packing. A higher compaction index implies a lower number of voids and a higher packing fraction of aggregates. 'K' value of 9 is used when a combination of vibration and compression is used to obtain the final aggregate mixture. The packing density Φ of the

mixture is related to the compaction index K using equation 1.

$$K = \sum_{i=1}^{n} \frac{y_i/\beta_i}{1/\Phi - 1/\gamma_i} \quad (1)$$

Here, y_i are the control parameters of the experiment and represent the individual packing fractions of the aggregates in the mixture. The residual packing density β_i represents the packing density of a mixture containing only the aggregate class 'i'. The values for residual packing density are determined experimentally using the dry rodded unit weight test. The virtual packing density γ_i is the theoretical value of packing density for the aggregate mixture when aggregate class 'i' is dominant. A dominant aggregate class is the one with the maximum volume fraction among all the other aggregate classes. Equation 1 can be solved numerically using Newton-Raphson method to obtain the packing density Φ once all the other parameters are determined using equations 2-4.

$$\gamma_i = \frac{\beta_i}{1 - \sum_{j=1}^{i-1}[1 - \beta_i + b_{ij}\beta_i(1 - 1/\beta_j)]y_j - \sum_{j=i+1}^{n}[1 - a_{ij}\beta_i/\beta_j]y_j} \quad (2)$$

Equation 2 is a linear formulation for the calculation of virtual packing density, which considers the interactions suffered by aggregate class 'i' due the presence of other aggregate classes. These interactions are in terms of the wall effect and the loosening effect. Loosening effect occurs when the packing density of a coarse grain mixture is decreased by the introduction of a fine grain (Fig. 12(a-b)). Wall effect is introduced when a coarse grain is immersed in a mixture consisting of fine grains and lowers the packing density of the mixture (Fig. 12(c-d)). In equation 2, a_{ij} and b_{ij} represent the loosening and wall effect coefficients respectively for aggregate class 'i' due to aggregate class 'j'.

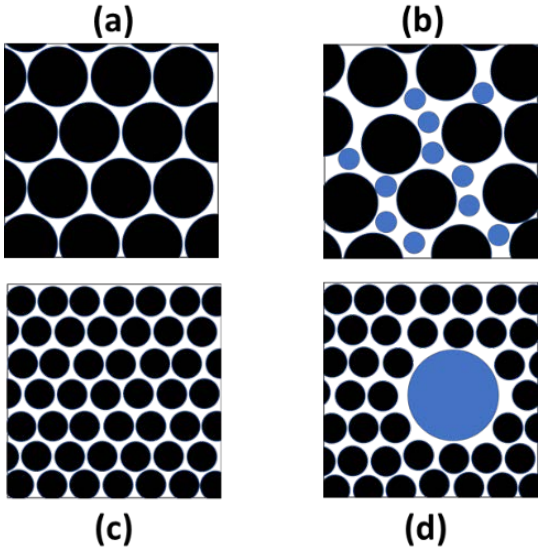

Fig. 12. (a-b) Densely packed mixture of coarse grains disturbed in the presence of fine grains showing loosening effect, (c-d) densely packed mixture of fine grains disturbed in the presence of a coarse grain illustrating wall effect.

While the calibration of model can be done by determining the a_{ij} and b_{ij} coefficients using experiments, a simplified empirical formulation has been shown to be a reasonable approximation of the experimental data. Both coefficients can be calculated as a function of the diameters d_i and d_j of aggregate classes 'i' and 'j' respectively.

$$a_{ij} = \sqrt{1 - \left(1 - d_j/d_i\right)^{1.02}} \quad (3)$$

$$b_{ij} = 1 - \left(1 - d_j/d_i\right)^{1.50} \quad (4)$$

4.3 Aggregate Optimization – Results

For UHPC to be used in larger volumes such as in bridge decks and piers, the use of coarser particles need to be considered to minimize volume changes and to reduce cost. The selection of appropriate aggregate gradation was done by optimizing the particle packing to obtain the maximum particle packing density in the known aggregate volume. For the UHPCs in this study, only three separate size ranges of coarse aggregates were considered – those with nominal maximum sizes of 6.25 mm, 4.75 mm and 2.36 mm. Two size ranges of fine aggregates – with d_{50} of 0.6 mm and 0.2 mm, were also chosen. The optimum fraction of individual aggregate classes required to achieve the maximum packing density was obtained by solving Equation 3 for multiple aggregate combinations. The volume fraction of each aggregate class was varied from 0.0 to 1.0 in increments of 0.1. This resulted in a total of 885 different aggregate combinations. A computer program was developed to automatically choose the aggregate combinations and input them into the algorithm for packing density determination. The distribution of the packing fraction as a function of the fraction of aggregate classes is given in Fig. 13 (a-b).

In Fig. 13 (a), the volume fraction of the coarse aggregate refers to the combined volume fraction of aggregates whose nominal maximum size exceeds 2.36 mm, which are the 6.25 mm, 4.75 mm and 2.36 mm nominal maximum size aggregates. Similarly, in Fig. 13 (b), fine aggregate refers to the two sands of median sizes 0.6 mm and 0.2 mm. In Fig. 13 (a), for each value of volume fraction of coarse aggregate on the x-axis, one can notice multiple values of the calculated packing density. These values correspond to the packing densities obtained by using different combinations of the chosen aggregates that result in a net coarse aggregate volume fraction equal to that shown on the x-axis. For instance, a coarse aggregate volume fraction of 0.60 may be achieved using multiple aggregate combinations of coarse aggregates (nominal maximum sizes of 6.25mm, 4.75mm, and 2.36 mm). Similarly, the fine aggregate volume fraction of 0.40 can be composed of different combinations of the two selected sizes of fine aggregates (d_{50} of 0.6 mm and 0.2 mm). As examples, the volume fractions of particles in a combined mixture containing 60% coarse aggregates

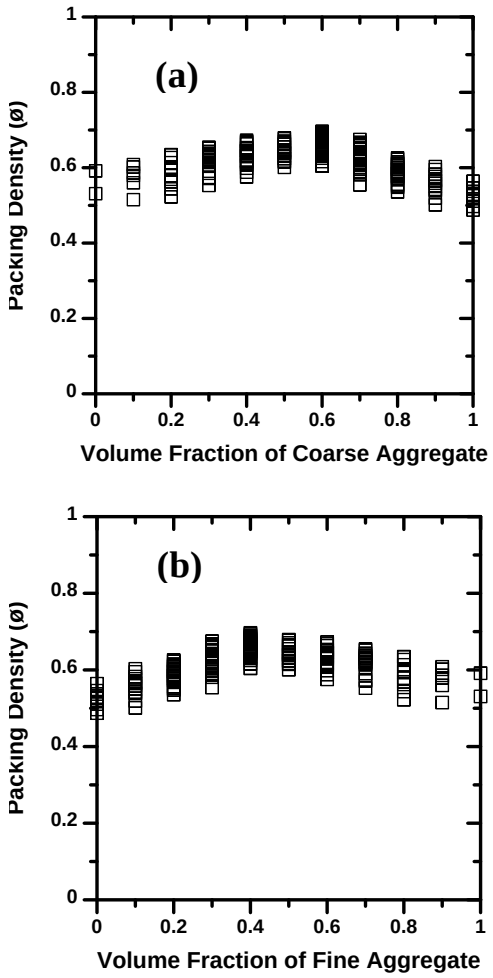

Fig. 13. Packing density as a function of volume fractions of: (a) coarse aggregate, (b) fine aggregate

and 40% fine aggregates, in the order of decreasing sizes, can be listed as (0.2,0.2,0.2,0.2,0.2), (0.4,0.1,0.1,0.2,0.2), (0.4,0.1,0.1,0.3,0.1) etc. Each of these combinations would result in a unique aggregate packing and therefore present a unique value of packing density.

It can be observed from Fig. 13 (a) that maximum packing density occurs when the volume fraction of coarse aggregates is 60%. The plot of packing density as a function of aggregate size combinations helps understand the combined effect of coarse and fine aggregates on the packing density of the mixture. A few results for packing fraction values calculated for combination of aggregate fractions are tabulated in Table 4. It is noted that the maximum value of packing fraction, ø is obtained as 0.696 for 40% fine aggregate, consisting of equal fractions of the 0.6 mm and the 0.2 mm sands, and 60% coarse aggregate, consisting of 40%, 10% and 10% fractions of 6.25 mm, 4.75 mm and 2.36 mm sized aggregates respectively. Such high degree of aggregate packing coupled with an optimized paste content is expected to lead to a dense concrete microstructure and subsequently result in lower porosity and higher strengths.

Table 4. Packing Fraction values for selected aggregate combinations. Italicized values are the optimum aggregate proportions determined

6.25 mm	4.75 mm	2.36 mm	Sand (0.6 mm)	Sand (0.2 mm)	Packing Fraction
0.4	0.1	0.1	0.2	0.2	0.696
0.6	0	0	0.2	0.2	0.690
0.3	0.1	0.2	0.2	0.2	0.685
0.1	0.3	0.1	0.3	0.2	0.675
0.5	0.1	0.1	0.2	0.1	0.671
0.1	0.3	0.2	0.3	0.1	0.657
0.2	0.1	0.4	0.1	0.2	0.634
0.1	0.1	0.1	0.2	0.5	0.599
0	0	0	0.6	0.4	0.591
0.2	0.1	0.5	0.1	0.1	0.587
0.4	0.1	0.5	0	0	0.546
0.1	0.1	0.8	0	0	0.494

Selected packing fraction values calculated were also verified using dry rodded unit weight testing. The aggregate combination with the highest packing fraction value was further selected for casting UHPC mixtures.

5.0 PROPERTIES OF SELECTED UHPC MIXTURES

5.1 Compression Strengths

Since all the three selected binders detailed in Table 2 showed comparable mortar compressive strengths as was shown in Fig. 4, two out of the three mixtures were selected for casting concrete cylinders and beam specimens. Two concrete batches were prepared for each binder mixture, one without any steel fibers and another incorporating 1% steel fiber by volume. The mixture proportions chosen for the concrete mixtures are given in Table 5.

The compressive strengths of concrete cylinders were measured using a 2670 kN load frame. Three cylinders each were tested after 7, 14 and 28 days of curing in a moist chamber and the average values are reported in Fig. 14. It was found that the compressive strength of all the specimens exceed 140 MPa at 28 days. The mixture containing fly ash, silica fume, and limestone, with an overall cement replacement level of 30%, was found to have the highest 28-day strength, of 153 MPa. Based on the mortar strength results shown in Fig. 11, this mixture can be expected to provide compressive strength in excess of 175 MPa after 56 or 90 days. The mixtures with fibers show comparable strengths as that of the mixtures without fibers, which is expected since 1% by volume of fibers do not contribute significantly to the compressive strength.

Table 5. – Mixture proportions for concrete mixtures. All the starting material contents, except the fiber content are relative masses with respect to that of the OPC

Mixture components	$F_{17.5}M_{7.5}L_5$	$F_{17.5}M_{7.5}L_5$-f	$M_{20}L_{30}$	$M_{20}L_{30}$-f
OPC	1.0	1.0	1.0	1.0
Fly Ash (FA)	0.175	0.175	-	-
Silica Fume (SF)	0.075	0.075	0.20	0.20
Limestone (LS)	0.05	0.05	0.30	0.30
HRWR	0.0125	0.0125	0.0127	0.0127
Steel Fibers (% by volume)	-	1.0	-	1.0
w/b (mass-based)	0.165	0.168	0.180	0.185
Aggregate/Binder	0.7	0.7	0.7	0.7

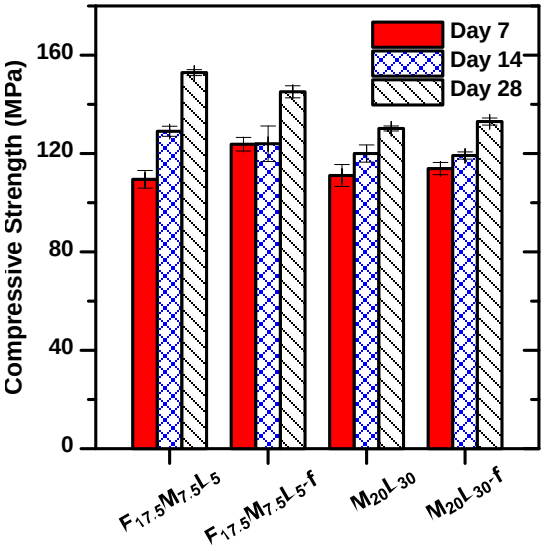

Fig. 14. Compressive strength of UHPC mixtures after 7, 14 and 28 days of curing

5.2 Ionic Transport

RCP and NSSM tests were used to determine the resistance of the UHP mixtures to chloride ion transport. Since both are electrically accelerated tests, the steel fiber reinforced mixtures were not considered. Fig. 15 compares the results for total charge passed for the UHPC mixtures during the RCP test with known values for regular OPC concrete (w/c = 0.40) and high-performance concrete (HPC; w/c = 0.32) obtained from previous studies (Neithalath and Jain, 2010; Poon *et al.*, 2006). The total charge passed during the RCP test is extremely low for the UHPC mixtures selected, attributable to the refinement of the pore structure through the use of a very low w/p and cement replacement materials, and the changes in pore solution conductivity primarily brought about by the use of silica fume. As per ASTM C 1202 classification, both the UHPC mixtures designed here fall under the “very low” rapid chloride permeability category.

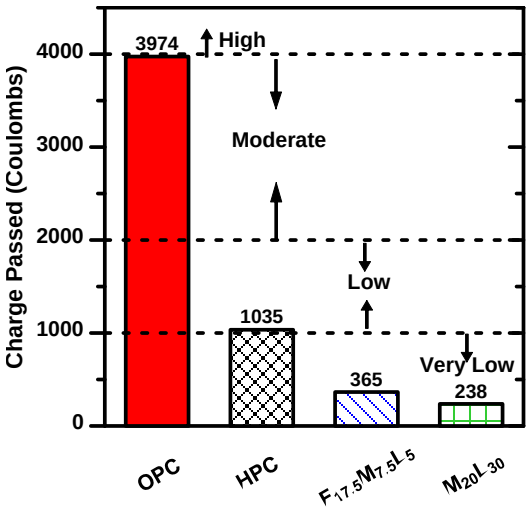

Fig. 15. Charge passed during the RCP test for the UHPC mixtures

The NSSM test carried out in accordance with NT Build 492 specifies different voltage values to be applied to the specimens based on the initial value of current under an applied voltage of 30 V (potential of 600 V/m). For UHPCs, because of the very dense microstructure, the initial current was very low, and thus a higher applied voltage of 60 V (1200 V/m potential) was needed. The NSSM coefficients for both the UHPC mixtures are shown in Fig. 16 along with the corresponding values for OPC concrete and HPC. The selected UHPCs have migration coefficients that are an order of magnitude lower than that of conventional OPC concrete. This has considerable implications in service-life of concrete structures designed using UHPCs.

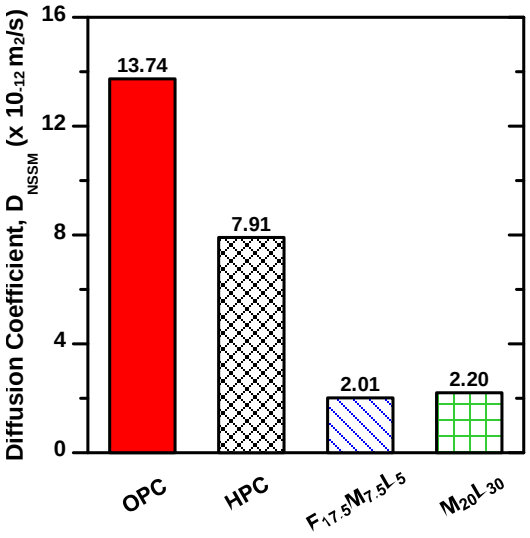

Fig. 16. Non-steady state migration coefficients (m^2/s) of the UHPC mixtures

6.0 CONCLUSIONS

This paper has described rational methodologies for the design of UHP concretes derived from the fundamental understanding of the characteristics of the component paste phase at the microstructure level and component aggregate phase at the mesostructure level. The ideal paste formulation suitable to exhibit ultra-high performance was selected from several binary, ternary, and quaternary blends using a stepwise algorithm that considered the effect of both microstructural packing as well as rheological properties of the binder. A microstructural packing algorithm was used to extract the mean centroidal spacing, number density, and the coordination number for the potential UHP pastes. The rheological parameters extracted include yield stress, plastic viscosity, and the mini-slump spread. Better packing allows improved utilization of cement replacement and filler materials, while better rheology facilitates better dispersion of particles and consequently improved mechanical properties. The microstructural and rheological parameters were utilized to create two different selection criteria. The first one was based on the individual microstructural or rheological parameters, and the second through the definition of packing and flow coefficients that expressed the combined effect of the chosen microstructural and rheological parameters. No relative weights were assigned for the microstructural and rheological parameters here, though it can be applied if needed. The proposed methodology allows the user to select mixtures based on acceptable ranges of microstructural packing and rheological parameters demanded by the application. The selected paste formulations were evaluated for the compressive strengths and 28-day compressive strengths close to 100 MPa were obtained for all mixtures.

In the next step, two quaternary binders containing fly ash or slag, microsilica, and limestone (for an overall cement replacement level of 30%), and one ternary binder containing microsilica and limestone (for an overall cement replacement level of 50%), were identified for detailed studies on UHPCs. While many UHPC studies only consider fine aggregates, this study considered three different sizes of coarse aggregates: nominal maximum size of 6.25 mm, 4.75 mm, and 2.36 mm, in addition to two different median sizes of fine aggregate: 0.6 mm and 0.2 mm. A compressible packing model was used for the packing of coarse and fine aggregates in UHPC. The influence of loosening and wall effects in poly-disperse mixtures was considered. A computer program analyzed 885 combinations of the three coarse and two fine aggregate sizes, and arrived at the combination with the densest packing (of 0.696). This combination consisted of 60% of coarse aggregates comprising of 40% of 6.25 mm size and 10% each of 4.75 mm and 2.36 mm aggregates. Highly flowable concretes (due to the rheology of the paste formulation) were proportioned using the chosen aggregate combination and two of the selected binders, with and without 1% of steel fibers by volume. 28-day compressive strengths in excess of 150 MPa were obtained. Significantly improved resistance to ionic transport as compared to conventional or high performance concretes was also observed, validating the material design procedure.

Acknowledgement

The authors sincerely acknowledge the Arizona Department of Transportation (ADOT) for funding this research (Grant no: SPR 745). The materials used for this study were provided by BASF Corporation, Salt River Materials Group, Holcim Cement, Burgess Pigments, and Omya A.G., and their contributions are acknowledged. This research was conducted in the Laboratory for the Science of Sustainable Infrastructural Materials at Arizona State University and the support that has made this laboratory possible is acknowledged. The contents of this paper reflect the views of the authors who are responsible for the facts and accuracy of the data presented herein, and do not necessarily reflect the views and policies of the funding agency, nor do the contents constitute a standard, specification, or a regulation.

References

Arora, A., Sant, G., and Neithalath, N. (2016). Ternary blends containing slag and interground/blended limestone: Hydration, strength, and pore structure. Constr. Build. Mater. *102*, *Part 1*, 113–124.

Arora, A., Aguayo, M., Mobasher, B., and Neithalath, N. Microstructural Packing- and Rheology-Based Binder Selection and Characterization for Ultra-High Performance Concrete (UHPC) [accepted for publication]. Cem. Concr. Res.

Burroughs, J.F., Shannon, J., Rushing, T.S., Yi, K., Gutierrez, Q.B., and Harrelson, D.W. (2017). Potential of finely ground limestone powder to benefit ultra-high performance concrete mixtures. Constr. Build. Mater. *141*, 335–342.

Chan, K.W., and Kwan, A.K.H. (2014). Evaluation of particle packing models by comparing with published test results. Particuology *16*, 108–115.

De Larrard, F. (1999). Concrete mixture proportioning: a scientific approach (CRC Press).

Ghafari, E., Costa, H., Júlio, E., Portugal, A., and Durães, L. (2014). The effect of nanosilica addition on flowability, strength and transport properties of ultra high performance concrete. Mater. Des. *59*, 1–9.

Ghafari, E., Arezoumandi, M., Costa, H., and Júlio, E. (2015). Influence of nano-silica addition on durability of UHPC. Constr. Build. Mater. *94*, 181–188.

Graybeal, B. (2011). FHWA TECHNOTE: Ultra High Performance Concrete. FHWA Publ. No FHWA-HRT-11-038 Fed. Highw. Adm.

Graybeal, B.A. (2012). Ultra-high performance concrete composite connections for precast concrete bridge decks (US Department of Transportation, Federal Highway Administration).

Huang, H., Gao, X., Wang, H., and Ye, H. (2017a). Influence of rice husk ash on strength and permeability of ultra-high performance concrete. Constr. Build. Mater. *149*, 621–628.

Huang, W., Kazemi-Kamyab, H., Sun, W., and Scrivener, K. (2017b). Effect of cement substitution by limestone on the hydration and microstructural development of ultra-high performance concrete (UHPC). Cem. Concr. Compos. *77*, 86–101.

de Larrard, F., and Sedran, T. (1994). Optimization of ultra-high-performance concrete by the use of a packing model. Cem. Concr. Res. *24*, 997–1009.

Le Hoang, A., and Fehling, E. (2017). Influence of steel fiber content and aspect ratio on the uniaxial tensile and compressive behavior of ultra high performance concrete. Constr. Build. Mater. *153*, 790–806.

Lee, N.K., Koh, K.T., Park, S.H., and Ryu, G.S. (2017). Microstructural investigation of calcium aluminate cement-based ultra-high performance concrete (UHPC) exposed to high temperatures. Cem. Concr. Res. *102*, 109–118.

Li, W., Huang, Z., Cao, F., Sun, Z., and Shah, S.P. (2015a). Effects of nano-silica and nano-limestone on flowability and mechanical properties of ultra-high-performance concrete matrix. Constr. Build. Mater. *95*, 366–374.

Li, Z., Venkata, H.K., and Rangaraju, P.R. (2015b). Influence of silica flour–silica fume combination on the properties of high performance cementitious mixtures at ambient temperature curing. Constr. Build. Mater. *100*, 225–233.

Maya, L.F., and Graybeal, B. (2017). Experimental study of strand splice connections in UHPC for continuous precast prestressed concrete bridges. Eng. Struct. *133*, 81–90.

Muhd Norhasri, M.S., Hamidah, M.S., Mohd Fadzil, A., and Megawati, O. (2016). Inclusion of nano metakaolin as additive in ultra high performance concrete (UHPC). Constr. Build. Mater. *127*, 167–175.

Neithalath, N., and Jain, J. (2010). Relating rapid chloride transport parameters of concretes to microstructural features extracted from electrical impedance. Cem. Concr. Res. *40*, 1041–1051.

Poon, C.S., Kou, S.C., and Lam, L. (2006). Compressive strength, chloride diffusivity and pore structure of high performance metakaolin and silica fume concrete. Constr. Build. Mater. *20*, 858–865.

Reda, M.M., Shrive, N.G., and Gillott, J.E. (1999). Microstructural investigation of innovative UHPC. Cem. Concr. Res. *29*, 323–329.

Roquier, G. (2016). The 4-parameter Compressible Packing Model (CPM) including a new theory about wall effect and loosening effect for spheres. Powder Technol. *302*, 247–253.

Russell, H.G., and Graybeal, B.A. (2013). Ultra-high performance concrete: A state-of-the-art report for the bridge community.

Shafieifar, M., Farzad, M., and Azizinamini, A. (2017). Experimental and numerical study on mechanical properties of Ultra High Performance Concrete (UHPC). Constr. Build. Mater. *156*, 402–411.

Soliman, N.A., and Tagnit-Hamou, A. (2017). Using glass sand as an alternative for quartz sand in UHPC. Constr. Build. Mater. *145*, 243–252.

Stovall, T., de Larrard, F., and Buil, M. (1986). Linear packing density model of grain mixtures. Powder Technol. *48*, 1–12.

Tazarv, M., and Saiidi, M.S. (2015). UHPC-filled duct connections for accelerated bridge construction of RC columns in high seismic zones. Eng. Struct. *99*, 413–422.

Van Tuan, N., Ye, G., van Breugel, K., and Copuroglu, O. (2011). Hydration and microstructure of ultra high performance concrete incorporating rice husk ash. Cem. Concr. Res. *41*, 1104–1111.

Vance, K., Aguayo, M., Oey, T., Sant, G., and Neithalath, N. (2013). Hydration and strength development in ternary portland cement blends containing limestone and fly ash or metakaolin. Cem. Concr. Compos. *39*, 93–103.

Vance, K., Arora, A., Sant, G., and Neithalath, N. (2015). Rheological evaluations of interground and blended cement–limestone suspensions. Constr. Build. Mater. *79*, 65–72.

Vikan, H., and Justnes, H. (2007). Rheology of cementitious paste with silica fume or limestone. Cem. Concr. Res. *37*, 1512–1517.

Vítek, J.L., Coufal, R., and Čítek, D. (2013). UHPC – Development and Testing on Structural Elements. Procedia Eng. *65*, 218–223.

Wang, C., Yang, C., Liu, F., Wan, C., and Pu, X. (2012). Preparation of Ultra-High Performance Concrete with common technology and materials. Cem. Concr. Compos. *34*, 538–544.

Wille, K., and Boisvert-Cotulio, C. (2015). Material efficiency in the design of ultra-high performance concrete. Constr. Build. Mater. *86*, 33–43.

Yoo, D.-Y., and Banthia, N. (2016). Mechanical properties of ultra-high-performance fiber-reinforced concrete: A review. Cem. Concr. Compos. *73*, 267–280.

Yu, R., Spiesz, P., and Brouwers, H.J.H. (2014). Mix design and properties assessment of Ultra-High Performance Fibre Reinforced Concrete (UHPFRC). Cem. Concr. Res. *56*, 29–39.